

Vessel Detection by Mean Shift Based Ray Propagation

Hüseyin Tek

Dorin Comaniciu

James P. Williams

Imaging and Visualization Department
Siemens Corporate Research, Inc.
755 College Road East, Princeton, NJ 08540
[{tek, comanici, williams}@scr.siemens.com](mailto:{tek,comanici,williams}@scr.siemens.com)

Abstract

A robust and efficient method for the segmentation of vessel cross-sections in contrast enhanced CT and MR images is presented. The primary innovation of the technique is the boundary propagation by mean shift analysis combined with a smoothness constraint. Consequently, the robustness of the mean shift to noise is enhanced by the use of apriori information on boundary smoothness. This processing is integrated into our computationally efficient framework based on ray propagation. The new algorithm allows real time segmentation of medical structures found in multi-modality images (CT, MR) and various examples are shown to illustrate its effectiveness.

1 Introduction

We focus on images produced by contrast-enhanced magnetic resonance angiography (CE-MRA) and computed tomography angiography (CTA.) In the CE-MRA imaging protocol, a contrast agent, usually based on the rare-earth element Gadolinium (Gd) (a highly paramagnetic substance), is injected into the bloodstream. In such images, blood vessels and organs perfused with the contrast agent appear substantially brighter than surrounding tissues. In CTA, a contrast agent is injected which increases the radio-opacity of the blood making the vessels appear dense. The goal of the majority of CTA/CE-MRA examinations is diagnosis and qualitative or quantitative assessment of pathology in the circulatory system. The most common pathologies are aneurysm and stenosis caused by arterial plaques. The modern clinical workflow for the reading of these images increasingly involves interactive 3D visualization methods, such as volume rendering for quickly pinpointing the location of the pathology. Once the location of the pathology is determined, quantitative measurements can be made on the original 2D slice data or, more commonly, on 2D multi planar reformat (MPR) images produced at user-selected positions and orientations in the volume. In the quantification of stenosis, it is desirable to produce a cross-sectional area/radius profile of a vessel so that one can compare pathological regions to patent (healthy) regions of the same vessel.

A basic problem in the segmentation of vessels from background is the accurate edge localization in the presence of noise. Most CT and MR images have significant noise levels. We employ one dimensional mean shift analysis along a set of rays projecting radially from a user-placed seed point in the image. Noise along these rays is eliminated while edges are preserved. The envelope of these rays represents an evolving contour which converges to the vessel lumen boundary. The algorithm is parsimonious, examining only pixels along and adjoining these rays and the seed point.

It is important that the boundary determined by the algorithm be consistent and invariant to medium to large scale linear and non-linear image inhomogeneities. This is needed for the algorithm to be insensitive to MR distortions. The use of constant threshold factors (such as Hounsfield-based thresholds in CT) would limit the ability of the algorithm to adapt to varying contrast dosages or varying beam energies in CT. We seek to localize the midpoint of the step-edge as the boundary of the vessel.

The choice of rise midpoint as the vessel lumen boundary is similar to the choice made by full-width-half-maximum (FWHM) segmentation methods [9]. It was, in fact, the sensitivity of conventional FWHM segmentation methods to noise which motivated the development of this method.

Our algorithm requires constant parameters for the evolution equations and for the window size used for the mean shift filter. To make the method adapt to varying image qualities and modalities, the evolution parameters are determined dynamically from the local statistics of the image computed from a small neighborhood immediately adjacent

to the users seed point. A limitation of our method as presented is that the detection scale is determined by user interaction. However, a fixed window size for the mean-shift filter will serve for detection over a broad range of vessel sizes.

There is an extensive body of work on the segmentation of vessels and other curvilinear structures (such as airways) from CTA and MRA images. Ray propagation has been used in a number of prior related works. Perhaps the most closely related example is the work of Wink et al. [24] who use image gradient to control ray termination. They use conventional smoothing techniques to deal with image noise. The drawback of such smoothing is that it can shift or entirely eliminate low-contrast boundaries.

Our approach is also related to other deformable models: snakes [11, 2, 3, 16, 25], balloons [7], levels-sets [14, 20, 22, 12, 20], region-competition [26], skeletally-coupled deformable models [18]. The position of this work in the deformable model taxonomy will be elaborated in Section 2.

In this paper we present the simplest usage case: The user specifies the vessel to be segmented by placing a single seed inside it. A boundary contour is then automatically generated via the propagation of rays from the seed point. The propagation is guided by image forces defined through mean shift analysis and smoothness constraints. The gradient-ascent mean shift localizes edges accurately in the presence of noise and provides a good computational performance, being based on local operators. The incorporation of a smoothness constraint into our model allows boundary finding in the presence of eccentricities like calcifications (CT) or small branching vessels. Also, the addition of smoothness constraints to our algorithm further improves the robustness to isolated noise. Although the algorithm is not optimized yet, it is very fast for detecting vessels in orthogonal views, under 0.5 seconds on a Pentium III , 500 Mhz PC.

This algorithm is also suitable for applications where multiple contours are to be segmented along a pre-determined vessel axis. In our integrated system we implement the axis extraction method described in [4] to provide orthogonal slice positions. Validation is vital to make this or any method useful in a clinical setting. In this paper examples are shown with phantoms of known ground truth and data from clinical practice. Complete validation will require a formal multi-site clinical test which is planned to begin within 6 months.

2 Active Contours

In this section we briefly review the “active contour” literature as is pertinent to this paper [11, 16, 7, 14, 20, 22, 4, 10, 24]. See also [26, 18] for related active contour methods for image segmentation.

2.1 Snakes

Active contours, or snakes [11, 3, 25], are deformable models based on energy minimization of controlled-continuity splines. When they are placed near the boundary of objects they will lock onto salient image features under the guidance of internal and external forces. Formally, let $\mathcal{C}(s) = (x(s), y(s))$ be the coordinates of a point on the snake, where s is the length parameter. The energy functional of a snake is defined as

$$E(\mathcal{C}) = \int_0^1 [E_{int}(\mathcal{C}(s)) + E_{image}(\mathcal{C}(s)) + E_{con}(\mathcal{C}(s))] ds, \quad (1)$$

where E_{int} represents the internal energy of the spline due to bending, E_{image} represents image forces, and E_{con} are the external constraint forces. First, the internal energy,

$$E_{int} = w_1 |\mathcal{C}'(s)|^2 + w_2 |\mathcal{C}''(s)|^2, \quad (2)$$

imposes regularity on the curve, and, w_1 and w_2 corresponds to elasticity and rigidity, respectively. Second, the image forces are responsible for pushing the snake towards salient image features. The local behavior of a snake can be studied by considering the Euler-Lagrange equation,

$$\begin{cases} -(w_1 \mathcal{C}')' + (w_2 \mathcal{C}'')'' = F(\mathcal{C}), \\ \mathcal{C}(0), \mathcal{C}'(0), \mathcal{C}(1) \text{ and } \mathcal{C}'(1) \text{ given,} \end{cases} \quad (3)$$

where $F(\mathcal{C})$ captures the image and external constraint forces. Note that the energy surface E is typically not convex and can have several local minima. Therefore, to reach the solution closest to the initialized snake, the associated dynamic problem is solved instead of the static problem. When the solution $\mathcal{C}(t)$ stabilizes, a solution to the static problem is achieved.

$$\begin{cases} \frac{\partial \mathcal{C}}{\partial t} - (w_1 \mathcal{C}')' + (w_2 \mathcal{C}'')'' = F(\mathcal{C}) \\ \text{initial + boundary conditions} \end{cases} \quad (4)$$

Snakes perform well when they are placed close to the desired shapes. However, a number of fundamental difficulties remain; in particular, snakes heavily rely on a proper initialization close to the boundary, multiple initializations, one per object of interest.

To overcome some of the initialization difficulties with snakes, Cohen and Cohen [7] introduced a deformable model based on the snakes idea. This models resembles a “balloon” which is inflated by an additional force which pushes the active contour to object boundaries, even when it is initialized far from the initial boundary. However, balloons still have some problems: First, like snakes, balloons cannot handle *topological changes*, i.e., merging and splitting. It should be noted that McInerney and Terzopoulos presented a topologically adaptable snakes in [15].

2.2 Level Set Evolution

One of the traditional problems of snakes and balloons is that they cannot easily capture topological changes. Therefore, for images with multiple objects, the snake or balloon methods require extensive user interaction. This problem can be resolved by the use of the level set evolution, proposed by Osher and Sethian for flame propagation [17], introduced to computer vision for shape representation [13], and first applied to active contours in [6, 14].

The level set approach consider a curve \mathcal{C} as the zero level set of a surface, $\phi(x, y) = 0$. Caselles *et al.* [6] proposed that the zero level set of the function ϕ , $\{x \in R^2 : \phi(t, x) = 0\}$, evolve in the normal direction according to

$$\frac{\partial \phi}{\partial t} = g(x, y)|\nabla \phi|(div(\frac{\nabla \phi}{|\nabla \phi|}) + v), \quad (5)$$

where $g(x, y) = \frac{1}{1+(\nabla G_\sigma * I)^2}$, v is a positive real constant, $G_\sigma * I$ is the convolution of the image I with the Gaussian G_σ , and, ϕ_0 is the initial data which is a smoothed version of the function $1 - X_\Gamma$, where X_Γ is the characteristic function of a set Γ containing the object of interest in the image. The gradient of the surface $\nabla \phi$ is the normal to the level set \mathcal{C} , \vec{N} , and the term $div(\frac{\nabla \phi}{|\nabla \phi|})$ is its curvature κ . Several interesting relevant approaches, *e.g.*, [12, 21] have been proposed after the original work of Caselles *et al.* [6], and Malladi *et al.* [14].

Unlike snakes, this active contour model is intrinsic, stable, *i.e.*, the PDE satisfies the maximum principle, and can handle topological changes such as merging and splitting without any computational difficulty. A key disadvantage of the level set method is their high computational complexity, due to the additional embedding dimensional, even when the computation is restricted to a narrow band around the curve. To overcome the computational complexity, narrow band level set evolutions have proposed [14, 1, 23]. However, these methods are still not fast enough for real-time image segmentation. Thus, in this paper, we propose to use ray propagation for fast image segmentation, which is described next.

3 Ray Propagation

Let the front be represented by a 2D curve $\mathcal{C}(s, t) = (x(s, t), y(s, t))$ where x and y are the Cartesian coordinates, s is the length parameter, and t is time. The evolution is then governed by [13]

$$\begin{cases} \frac{\partial \mathcal{C}(s, t)}{\partial t} = c(x, y)\vec{N} \\ \mathcal{C}(s, 0) = \mathcal{C}_0(s) \end{cases} \quad (6)$$

where $\mathcal{C}_0(s) = (x(s, 0), y(s, 0))$ is the initial curve, and \vec{N} is the unit normal vector and $c(x, y)$ is the speed of a ray at point (x, y) .

The approach that we consider in this paper is based on explicit front propagation via normal vectors. Specifically, the contour is sampled and the evolution of each sample is followed in time by rewriting the Eikonal equation [19] in vector form, namely,

$$\begin{cases} x_t(s, t) = c(x, y)\frac{y_s}{\sqrt{x_s^2+y_s^2}} \\ y_t(s, t) = c(x, y)\frac{x_s}{\sqrt{x_s^2+y_s^2}}. \end{cases} \quad (7)$$

This evolution is the “Lagrangian” solution since the physical coordinate system moves with the propagating wavefront. However, the applications of ray propagation for curve evolution has been limited. Because when the normals to the wavefront collide (formation of shocks), this approach exhibits numerical instabilities due to an accumulated density of sample points, thus requiring special care, such as reparametrization of the wavefront. Also, topological changes are not handled naturally, *i.e.*, an external procedure is required.

In this paper, we will show that ray propagation can in fact be used for segmenting certain objects in medical images efficiently and robustly. Previously, ray propagation has been used to implement *full-width at half-maximum* (FWHM) technique for quantification of 2D airway geometry [9]. In FWHM technique, the maximum and minimum intensity values along the rays are computed to determine the “half-maximum” intensity value, which is the half intensity value between maximum and minimum. However, stable computation of maximum and minimum along the rays are quite difficult due to high signal variations.

In addition, ray propagation was used by Wink *et al.* [24] for fast segmentation of vessels and detection of their centerline. In this approach, Wink *et. al.* used the intensity gradients to stop the propagation of rays. However, this approach faces difficulties when the vessels boundaries are not sharp, *i.e.*, due to partial volume effects, and also when vessels contain isolated noises, *e.g.*, calcifications in CT images.

The main shortcomings of these approaches stem from the computation of image gradients which are not robust relative to the image noise. In this paper, we propose to use *mean shift* analysis for detecting vessels boundaries efficiently and robustly. Comaniciu and Meer [8] showed that the image discontinuities are robustly revealed by a mean shift process which evolves in both the intensity and image space.

We will first describe the mean shift analysis; second, illustrate an approach where the mean shift procedure is applied to select discontinuities in a one dimensional signal; and finally, present the mean shift-based ray propagation approach for segmentation of medical structures, *e.g.*, vessels.

3.1 Mean Shift Analysis

Given the set $\{\mathbf{x}_i\}_{i=1\dots n}$ of d -dimensional points, the mean shift vector computed at location \mathbf{x} is given by [8]

$$M_h(\mathbf{x}) = \frac{\sum_{i=1}^n \mathbf{x} K(\frac{\mathbf{x}-\mathbf{x}_i}{h})}{\sum_{i=1}^n K(\frac{\mathbf{x}-\mathbf{x}_i}{h})} - \mathbf{x} \quad (8)$$

where K represents a kernel with a monotonically decreasing profile and h is the bandwidth of the kernel.

It can be shown that (8) represents an estimate of the normalized density gradient computed at location \mathbf{x} , i.e., the mean shift vector always points towards the direction of the maximum increase in the density. As a result, the successive computation of expression (8), followed by the translation of the kernel K by $M_h(\mathbf{x})$ will define a path that converges to a local maximum of the underlying density. This algorithm is called the *mean shift procedure*, a simple and efficient statistical technique for mode detection.

The mean shift procedure can be applied for the data points in the joint *spatial-range* domain [8], where the space of the 2-dimensional lattice represents the *spatial* domain and the space of intensity values constitutes the *range* domain. In this approach, a data point defined in the joint spatial-range domain is assigned with a point of convergence which represents the local mode of the density in this space, *e.g.*, a 3-dimensional space for gray level images. One can define displacement vector in the spatial domain as the spatial difference between convergence point and the original point.

When each pixel in the image is associated with the new range (intensity) information carried by the point of convergence, the algorithm produces discontinuity preserving smoothing. Conceptually, this process is similar to the anisotropic diffusion, nonlinear filtering, or bilateral filtering [5].

However, when the spatial information corresponding to the convergence point is also exploited, one can define a segmentation process based on the displacement vectors of each pixel. The convergence points sufficiently close in this joint domain are gathered together to form uniform regions for image segmentation [8].

In this paper, we will exploit the mean shift-generated displacement vectors to guide active contour models. The robustness of the mean shift is thus combined with *a priori* information regarding the smoothness of the object contours. This processing is integrated into our computationally efficient framework based on ray propagation. The new algorithm allows real time segmentation of medical structures.

3.2 Mean Shift Filtering Along a Vector

Let us first illustrate the mean shift procedure applied to a 1-dimensional intensity profile which is obtained from a 2d gray level image. Specifically, let $\{x_i, I_i\}_{i=1,\dots,N}$ and $\{x^*_i, I^*_i\}_{i=1,\dots,N}$ be the 2-dimensional original and filtered N image points in the spatial-range domain. In addition, the output of the mean-shift filter includes a displacement vector $\{d_i\}_{i=1,\dots,N}$ which measures the spatial movement of each spatial point. In our algorithm, each point in this spatial-range domain is processed via the mean shift operator until convergence. Specifically, the algorithm consists of 3 steps:

For each $i = 1, \dots, N$

1. Initialize $k = 1$ and $(x^{*k}_i, I^{*k}_i, d_i) = (x_i, I_i, 0)$
2. Compute

$$\begin{aligned} x^{*k+1}_i &= \frac{\sum_{j=1}^M x_j e^{-\frac{(x^{*k}_i - x_j)^2}{2\sigma_x^2}}}{\sum_{j=1}^M e^{-\frac{(x^{*k}_i - x_j)^2}{2\sigma_x^2}}} \frac{-\frac{(I^{*k}_i - I_j)^2}{2\sigma_I^2}}{e^{-\frac{(I^{*k}_i - I_j)^2}{2\sigma_I^2}}} \\ I^{*k+1}_i &= \frac{\sum_{j=1}^M I_j e^{-\frac{(x^{*k}_i - x_j)^2}{2\sigma_x^2}}}{\sum_{j=1}^M e^{-\frac{(x^{*k}_i - x_j)^2}{2\sigma_x^2}}} \frac{-\frac{(I^{*k}_i - I_j)^2}{2\sigma_I^2}}{e^{-\frac{(I^{*k}_i - I_j)^2}{2\sigma_I^2}}} \end{aligned} \quad (9)$$

until the displacement of spatial points, x_i are small, *i.e.*, $|x^{*k+1}_i - x^{*k}_i| < \epsilon$

3. Assign $d_i = (x^{*k+1}_i - x_i)$
4. Assign $(x^*_i, I^*_i) = (x_i, I_i)$

where σ_x and σ_I determine the Gaussian spatial and range kernels size, respectively. Observe that in the last step of the procedure the original spatial locations, namely x_i 's are assigned with the smoothed intensity values. Figure 1a illustrates an example where 1-dimensional intensity data is obtained from a slice of a CT image. Figure 1b and c illustrate the original intensity profile and the smoothed intensity profile, respectively. Observe that the mean shift procedure smooths the intensity data while preserving and sharpening its discontinuities. Similarly, Figure 1d depicts the displacement vectors along this 1-dimensional signal. Our boundary detection framework exploits the information contained in these displacement vectors.

3.3 Mean Shift-Based Ray Propagation

Semi-automatic segmentation procedures are very well-accepted in medical image applications because of their fast execution times and their stability. Infact, active contours have been extensively used in medical image segmentation. In this paper, we advocate ray propagation from a

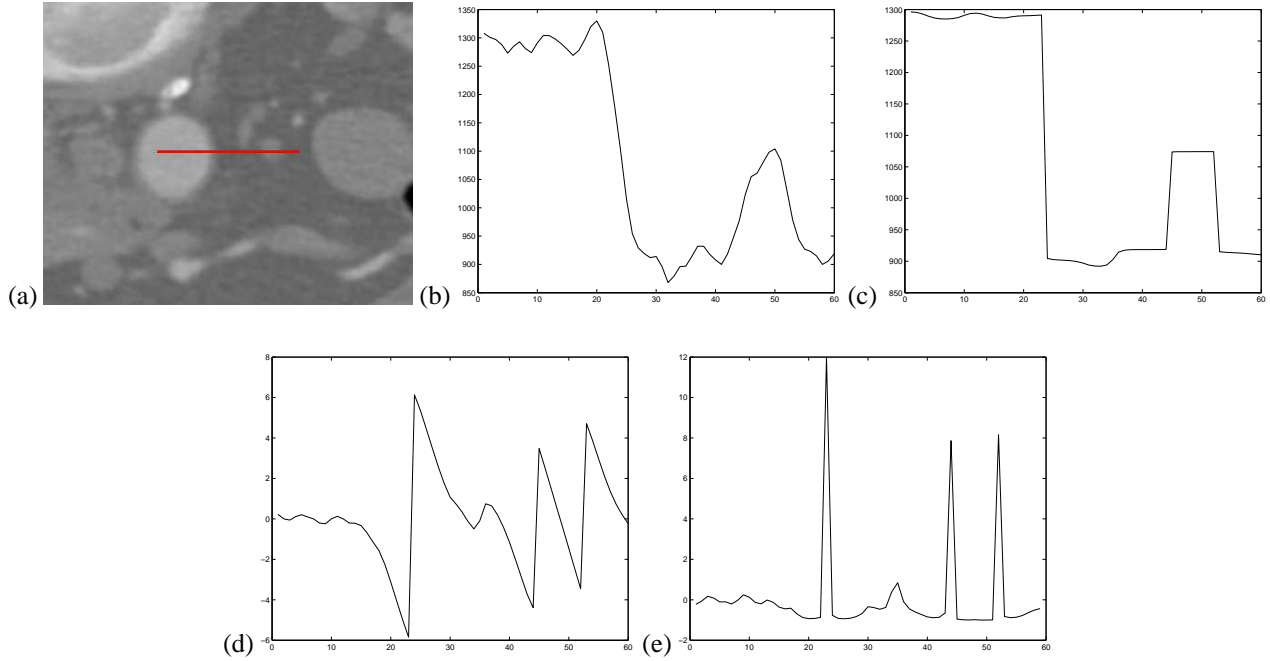


Figure 1. (a) A 1-dimensional intensity profile is obtained along the red line from a CT image containing the aorta. The left-end point of the red line is the beginning of data and right-end point is the end of data. (b) Original intensity profile. (c) Intensity profile after mean shift filtering, with $\sigma_x = 3$ and $\sigma_I = 100$. (d) The displacement vectors of each spatial point and their first derivatives (e).

single point for vessel segmentation. Specifically, we assume that the vessels are orthogonal to the viewing plane and their boundaries are very similar to circular/elliptical objects. Thus, ray propagation is very well suited for this problem for the following reasons. First, ray propagation is very fast. Second, no topological changes are necessary and no shocks form during the propagation, since rays from a single source point do not collide with each other. Recall that level sets have been the choice of curve evolution problems [13] due to formation of shocks and topological changes that may happen during the evolution. However, based on our experiments, level set based segmentation techniques, *e.g.*, [14, 21] are still slow for real time image segmentation.

Let us now present the mean shift based ray propagation: The approach is based on an explicit front propagation via normal vectors, *rays*. Specifically, the evolving contour is sampled and the evolution of each sample is followed in time by rewriting the evolution equation in vector form, namely,

$$\begin{cases} x_t(s, t) = S(x, y) \frac{y_s}{\sqrt{x_s^2 + y_s^2}} \\ y_t(s, t) = S(x, y) \frac{x_s}{\sqrt{x_s^2 + y_s^2}} \end{cases} \quad (10)$$

where $S(x, y)$ is a speed function defined as

$$S(x, y) = \alpha \frac{f(x, y)}{1.0 + |\nabla d(x, y)|^2} + \beta \kappa(x, y) \quad (11)$$

where $d(x, y)$ is the displacement function computed by the mean shift procedure, $\kappa(x, y)$ is the discrete curvature, α and β are constants, and $f(x, y)$ is given by

$$f(x, y) = \begin{cases} -\text{sign}(d(x, y)) & \text{if } |\nabla d(x, y)| > 3\sigma_d \\ 1 & \text{else} \end{cases} \quad (12)$$

Ideally, rays should propagate freely towards the object boundaries when they are away from them and they should slow down in the vicinity of these object boundaries. If they cross over the boundaries they should come back to the boundary. Observe that all these requirements are satisfied by the choice of speed function. The mean shift-generated displacement vectors have high gradient magnitude (Figure 1e) and diverge (Figure 1d) at the aorta boundary. Note that the high gradient magnitude results in low propagation speed, while the divergence property determines the direction of the propagation, *i.e.*, outward inside the aorta and inward outside the aorta.

Often intensity values inside vessels are not smoothly changing. In fact, it is possible that there may be isolated

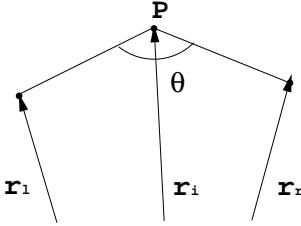


Figure 2. The curvature of a ray r_i at P is approximated by the angle θ at that vertex.

noise which then creates severe problems for the propagation of rays. In addition, the object boundaries may be distorted at isolated locations due to interaction with nearby structures. Because of these irregularities inside vessels and on its boundaries, we believe that there must be some smoothness constraints on the evolving contour via rays. Thus, we add $\kappa(x, y)$ to the speed function of rays, which forces the front to be smooth during the propagation. We currently use $\kappa(x, y) = (1 - (\frac{\theta}{\pi})^2)$ as the curvature value of a ray at point (x, y) where θ is the angle between two contour segments, Figure 2. The ratio α/β controls the degree of desired smoothness.

Our speed function contains the σ_d parameter. This statistical parameter is the variation of the magnitude of displacement function in a region and is learned from the data. Specifically, first rays are initially propagated via constant speed in a small region (circular region). Second, first order statistics, namely, mean, μ and standard deviation, σ_d of gradient displacement function are computed from this sample. It is assumed that locations of the small gradients in a displacement function (less than $3\sigma_d$) should not be part of any object boundary.

4 Results

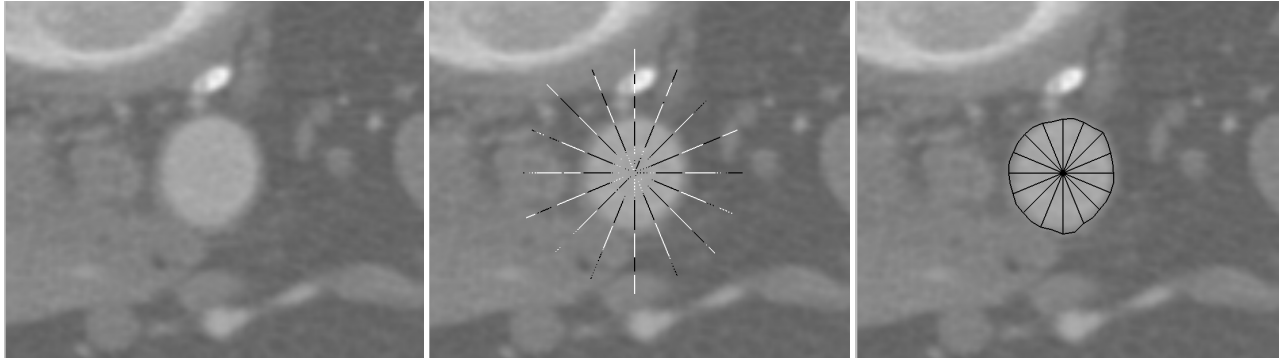
Figure 3 illustrates the mean shift-based ray propagation for a CT (top) and a MR image (bottom). Specifically, we depict the displacement vectors obtained from mean shift filtering in middle column in order to show the strength of the mean shift filtering. In this figure, black color indicates a vector pointing towards the center and similarly white colors are the vectors pointing outward from the center of rays. Observe the divergence of the displacement vectors in the vicinity of aorta boundaries. This divergence of vectors are integrated via rays, which then leads to the segmentation of aorta.

We have tested the stability of our algorithm on a variety of CT and MR images and as well as on a CT phantom data, Figure 4. Further validation studies will be done by the experts.

Figure 5 illustrates the need for shape priors, e.g., smoothness constraints in segmentation on an MR image and a CT image. Shape priors are necessary for two reasons: (i) Figure 5a depicts a case where renal arteries branch from the aorta. The segmentation of aorta for quantitative measurements via ray propagation without any smoothness constraint would result in large errors due to renal arteries, Figure 5b. The addition of strong smoothness constraint results in better segmentation of aorta for quantitative measurements, Figure 5c. This example illustrates that our algorithm is capable of incorporating simple shape priors. (ii) The smoothness constraint is often needed for the stability of a segmentation process. Figure 5a illustrates a structure in a CT image which has diffused boundaries and a circular dark region in it. Observe that the ray passing over the circular dark region is stopped due to the high displacement vector (or high intensity gradient), Figure 5b. In addition, one ray did not stop at the correct boundary due to the very low gradient. Figure 5c illustrates that these isolated errors in the segmentation process can be corrected by the addition of smoothness constraints.

References

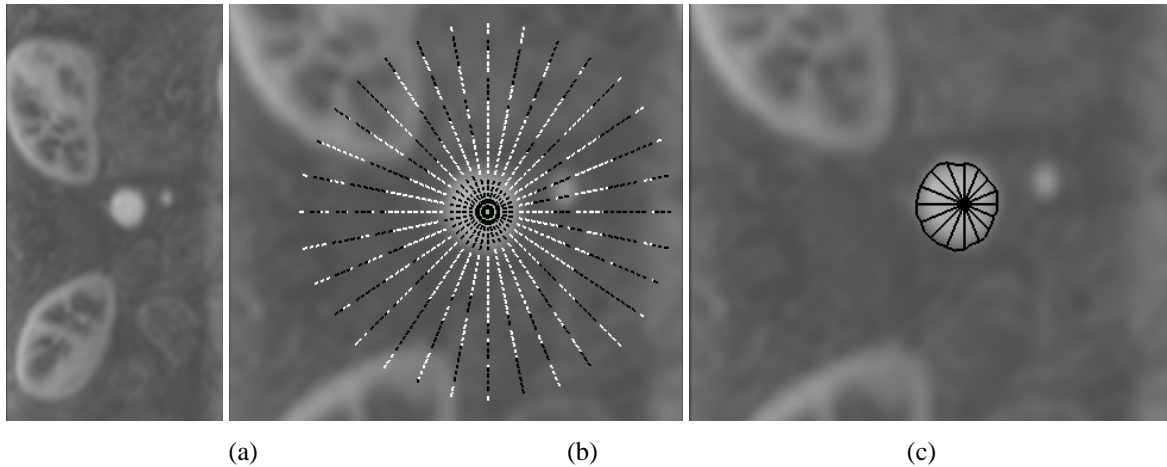
- [1] D. Adalsteinsson and J. Sethian. A fast level set method for propagating interfaces. *J. Comput. Phys.*, 118:269–277, 1995.
- [2] A. Amini, S. Tehrani, and T. Weymouth. Using dynamic programming for minimizing the energy of active contours in the presence of hard constraints. In *International Conference on Computer Vision, Tampa, Florida*, pages 95–99, 1988.
- [3] A. Amini and T. Weymouth. Using dynamic programming for solving variational problems in vision. *IEEE Trans. Pat. Analysis and Machine Intelligence*, 12(9):855–867, 1990.
- [4] B. B. Avants and J. P. Williams. An adaptive minimal path generation technique for vessel tracking in CTA/CE-MRA volume images. In *Medical Image Computing and Computer-Assisted Intervention MICCAI*, pages 707–716, 2000.
- [5] D. Barash. Bilateral filtering and anisotropic diffusion: Towards a unified viewpoint. Technical Report HPL-2000-18(R.1), Hewlett-Packard, 2000.
- [6] V. Caselles, F. Catte, T. Coll, and F. Dibos. A geometric model for active contours in image processing. Technical Report No 9210, CEREMADE, 1992.
- [7] L. D. Cohen. Note on active contour models and balloons. *CVGIP: Image Understanding*, 53(2):211–218, 1991.
- [8] D. Comaniciu and P. Meer. Mean shift analysis and applications. In *IEEE International Conference on Computer Vision*, pages 1197–1203, 1999.
- [9] N. D. D’Souza, J. M. Reinhardt, and E. A. Hoffman. ASAP: Interactive quantification of 2d airway geometry. In *Meical Imaging 1996: Physiology and function from Multidimensional Images, Proc. SPIE 2709*, pages 180–196, 1996.



(a)

(b)

(c)



(a)

(b)

(c)

Figure 3. This figure illustrates the mean shift-based ray propagation on a CT (top) and MR image aorta (bottom). Both images contain aorta. (Right) Original image (Middle) The unit displacement vectors of mean shift procedure are computed via propagating unit speed rays, *i.e.*, speed function is unity. The white indicates a vector pointing outward from the center and black color indicates a vector pointing towards the center. Observe that our speed function in Equation (12) includes the negative sign of the displacement vectors. Thus initially rays are pushed towards to the vessels boundaries and if they cross over them they come back due to sign change in the speed function. (Right) The segmentation of vessel via mean shift-based ray propagation.

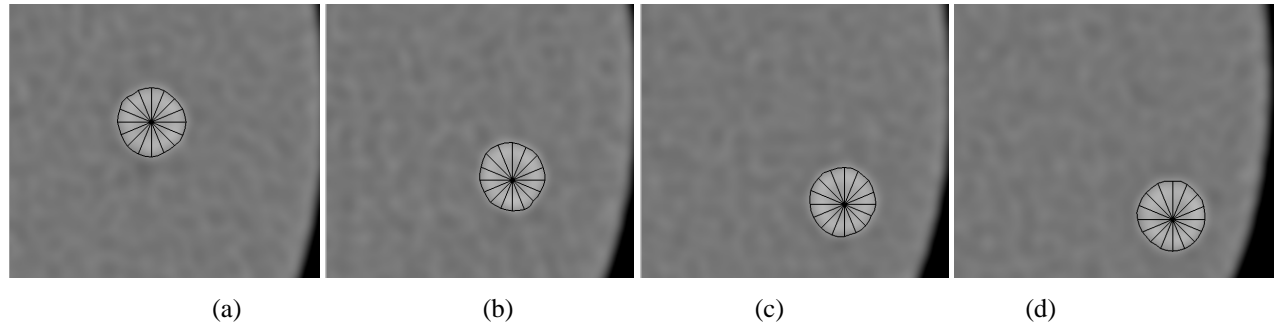


Figure 4. This example illustrates the stability of our results on a CT phantom data depicting coronary arteries. The boundaries are detected by a single click inside the vessels.

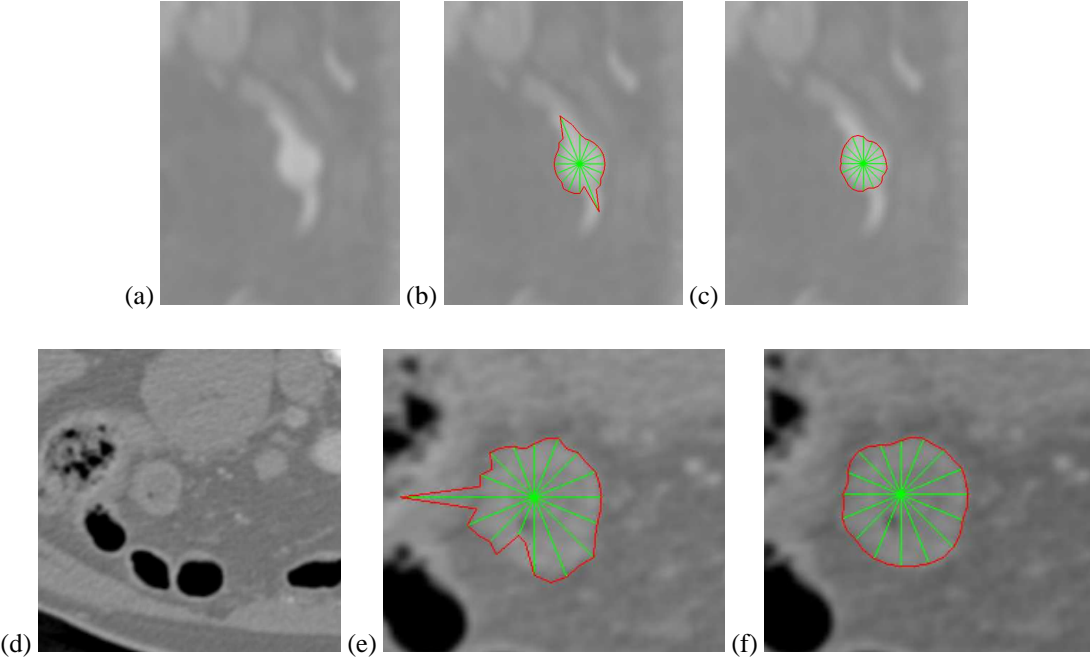


Figure 5. This figure illustrates the need for a smoothness constraint in segmentation on an MR image and a CT image. (Left) Original image. (Middle) Boundary detection by mean shift-based ray propagation without any shape priors. (Right) Boundary detection by mean shift based ray propagation with smoothing constraints. Observe that (e) and (f) depicts a zoomed area of the original image shown in (d).

- [10] M. Hernandez-Hoyos, A. Anwander, M. Orkisz, J. P. Roux, and I. E. M. P. Doueck. A deformable vessel model with single point initialization for segmentation, quantification and visualization of blood vessels in 3D MRA. In *MICCAI'00*, pages 735–745, 2000.
- [11] M. Kass, A. Witkin, and D. Terzopoulos. Snakes: active contour models. *International Journal of Computer Vision*, 1(4):321–331, 1988.
- [12] S. Kichenassamy, A. Kumar, P. Olver, A. Tannenbaum, and A. Yezzi. Gradient flows and geometric active contour models. In *Fifth International Conference on Computer Vision*, pages 810–815, 1995.
- [13] B. B. Kimia, A. R. Tannenbaum, and S. W. Zucker. Shapes, shocks, and deformations, I: The components of shape and the reaction-diffusion space. *IJCV*, 15:189–224, 1995.
- [14] R. Malladi, J. A. Sethian, and B. C. Vemuri. Shape modelling with front propagation: A level set approach. *IEEE Transactions on Pattern Analysis and Machine Intelligence*, 17, 1995.
- [15] T. McInerney and D. Terzopoulos. Topologically adaptable snakes. In *IEEE International Conference on Computer Vision*, pages 840–845, 1995.
- [16] T. McInerney and D. Terzopoulos. Deformable models in medical images analysis: a survey. *Medical Image Analysis*, 1(2):91–108, 1996.
- [17] S. Osher and J. A. Sethian. Fronts propagating with curvature dependent speed: Algorithms based on Hamilton-Jacobi formulations. *Journal of Computational Physics*, 79:12–49, 1988.
- [18] T. B. Sebastian, H. Tek, J. J. Crisco, S. W. Wolfe, and B. B. Kimia. Segmentation of carpal bones from 3d CT images using skeletally coupled deformable models. In *MICCAI*, pages 1184–1194, 1998.
- [19] J. A. Sethian. *Level Set Methods*. Cambridge University Press, New York, 1996.
- [20] J. Shah. A common framework for curve evolution, segmentation and anisotropic diffusion. In *IEEE Conference on Computer Vision and Pattern Recognition*, 1996.
- [21] K. Siddiqi, A. Tannenbaum, and S. Zucker. Area and length minimizing flows for image segmentation. *IEEE Trans. Image Processing*, 7:433–444, 1998.
- [22] H. Tek and B. B. Kimia. Image segmentation by reaction-diffusion bubbles. In *IEEE International Conference on Computer Vision*, pages 156–162, 1995.
- [23] R. Whitaker. Algorithms for implicit deformable models. In *ICCV95*, pages 822–827, 1995.
- [24] O. Wink, W. Niessen, and M. A. Viergever. Fast delineation and visualization of vessels in 3-D angiographic images. *IEEE Trans. on Medical Imaging*, 19:337–345, 2000.
- [25] C. Xu and J. Prince. Snakes, shapes, and gradient vector flow. *IEEE Trans. Image Proc*, pages 359–369, 1998.
- [26] S. C. Zhu and A. L. Yuille. Region competition: Unifying Snakes, Region growing, and Bayes/MDL for multiband Image Segmentation. *PAMI*, 18(9):884–900, 1996.